

Freezing transition of hard hyperspheres

Reimar Finken,¹ Matthias Schmidt,² and Hartmut Löwen²

¹*University Chemical Laboratory, Lensfield Road, Cambridge CB2 1EW, United Kingdom*

²*Institut für Theoretische Physik II, Heinrich-Heine-Universität Düsseldorf, Universitätsstraße 1, 40225 Düsseldorf, Germany*

(Received 22 May 2001; published 14 December 2001)

We investigate the system of D -dimensional hard spheres in D -dimensional space, where $D > 3$. For the fluid phase of these hyperspheres, we generalize scaled-particle theory to arbitrary D and furthermore use the virial expansion and the Percus-Yevick integral equation. For the crystalline phase, we adopt cell theory based on elementary geometrical assumptions about close-packed lattices. Regardless of the approximation applied, and for dimensions as high as $D = 50$, we find a first-order freezing transition, which preempts the Kirkwood second-order instability of the fluid. The relative density jump increases with D , and a generalized Lindemann rule of melting holds. We have also used ideas from fundamental-measure theory to obtain a free energy density functional for hard hyperspheres. Finally, we have calculated the surface tension of a hypersphere fluid near a hard smooth (hyper-)wall within scaled-particle theory.

DOI: 10.1103/PhysRevE.65.016108

PACS number(s): 64.60.Cn, 64.70.Dv, 61.20.Gy

I. INTRODUCTION

In the last decades, our understanding of the freezing transition has greatly advanced [1,2]. Most of the success comes from the insight that the essential molecular mechanism that drives freezing can be understood in terms of different kinds of entropy [3]. This is demonstrated by ordering transitions that purely entropy-driven hard-core particles exhibit. The simple model of hard spheres, which has only the sphere packing fraction as thermodynamical parameter, has played a key role in a statistical description of freezing; for a recent review see [4]. Computer simulations [5,6] have shown that there is a first-order freezing transition from a fluid into a face-centered-cubic crystal at a packing fraction of around 0.5 with a relative density jump across freezing of about 10%. In two spatial dimensions (hard discs), the precise nature of freezing is still a matter of debate but there is recent evidence from computer simulations that the transition is in accordance with the Kosterlitz-Thouless scenario [7]. The thermodynamics of the one-dimensional model, namely, hard rods, can be calculated analytically [8] revealing that there is no freezing transition at packing fractions away from close packing.

From a more theoretical point of view, it is interesting to study systems in spatial dimension D higher than three. The motivation to do so is twofold. First, the limit of infinite dimension may lead to enormous simplifications allowing sometimes even for an analytical solution of the thermodynamics, fluid structure, and phase transformations. Recent examples include the hypercube [9] and hypersphere [10] fluid, the lattice plasma [11], the Gaussian potential [12,13] as well as systems with attractions [14,15]. The advantage in high dimensions is that the third and higher virial coefficients vanish asymptotically. Once the limit $D \rightarrow \infty$ is known, it may serve as a reference system in order to include finite dimensions in a perturbative analysis as a function of $1/D$, see e.g., Refs. [13,16] for such discussions. Second, the crossover between different spatial dimensions imposes physical consistency constraints on the theories. Understanding a fluid in different dimensions is important for constructing, e.g., density functionals explicitly. For hard spheres, ap-

proximate functionals can be obtained by imposing the correct crossover to reduced D . This idea was exploited particularly in the construction of fundamental-measure density functionals [17,18] in dimensions $D = 2, 3$ [19–21].

Systems composed of hard hyperspheres, being the natural extension of hard spheres to arbitrary spatial dimensions D , have, therefore, been considered quite extensively. The limit of infinite dimensions was studied in relation to the thermostatics [10,22,24,23,13] and dynamics [25]. Furthermore, the third and fourth virial coefficients have been calculated for arbitrary dimensions [26], and different fluid state theories for the thermodynamics and structure proposed based either on an overlap volume approach [27], the Percus-Yevick [28], mean spherical [29], or hypernetted chain [30] approximation. For $D = 4, 5$, a crystalline phase of hyperspheres has been studied with free-volume theory [31], the freezing transition has been examined by computer simulation [32], and density functional theory [33]. Furthermore, the demixing transition in a binary hypersphere mixture has been discussed [34,35] on the basis of a Carnahan-Starling-type equation of state [36,37].

In this paper we investigate the freezing transition of hyperspheres in *arbitrary* dimension, which has not been addressed until now. This aim requires a detailed description for the free energies of the fluid and solid state. For the fluid free energy, we use several methods such as the virial expansion, scaled-particle theory, fundamental-measure density functional, and the Percus-Yevick liquid-integral equation. All these approaches feature the exact second virial coefficient. For large dimensions, higher-order contributions are known to vanish, and consequently we obtain similar fluid free energies from all approaches. To access the free energy of the solid, we use the free-volume theory together with geometric results about the close-packed density and the structure of so-called laminated lattices in high dimension. In contrast to earlier approaches based on a fluid instability analysis [13,23], we obtain a first-order freezing transition even for high dimensions. We show that the freezing transition preempts this Kirkwood-type second-order spinodal instability of the fluid. The relative density jump across freezing even increases with rising dimension D . The Lindemann

parameter at melting is very robust with respect to a change of dimensionality such that the Lindemann rule of melting can be carried over to arbitrary dimensions. As a side product of scaled-particle theory, we derive an analytical expression for the surface tension between a smooth hard (hyper-)wall and a hard hypersphere fluid for any D . Furthermore, we develop a density functional for arbitrary spatial dimension in the spirit of Rosenfeld's fundamental-measure theory [17–21].

The paper is organized as follows. In Sec. II, we briefly summarize mathematical properties of close-packing densities. The solid free energy is outlined in Sec. III. In Sec. IV, we describe different approaches to the fluid free energy. Section V is devoted to the construction of a density functional for inhomogeneous hard hyperspheres. Results for freezing are presented in Sec. VI, and we finally conclude in Sec. VII.

II. HYPERSPHERES, LATTICES, AND CLOSE PACKING

The interaction between hard hyperspheres is pairwise and given by the potential

$$u(r) = \begin{cases} \infty, & r < 2R \\ 0, & r \geq 2R, \end{cases} \quad (1)$$

where r is the Euclidian center-to-center separation in D dimensions and R denotes the hypersphere radius. Thermodynamical and structural properties of the hard hypersphere system are independent of temperature T , which only sets the energy scale $k_B T \equiv 1/\beta$. The system's only relevant parameter is the number density ρ , measuring the number of particles per D -dimensional volume. A suitable dimensionless packing fraction is defined via $\eta = \rho V_D(R)$, where $V_D(R) = R^D \pi^{D/2} / \Gamma(1 + D/2)$ denotes the D -dimensional volume of the hypersphere of radius R and $\Gamma(x)$ is the gamma function. To simplify the notation, we denote the volume of the unit sphere of radius $R=1$ as $V_D \equiv V_D(1)$. We also define the $(D-1)$ -dimensional surface as $s_{D-1}(R) = D V_D R^{D-1}$.

Due to packing constraints, η has a D -dependent upper limit, which is the so-called close-packing fraction η_{cp} . The value of η_{cp} is known in a mathematically rigorous sense only in the cases $D=1,2,3$, see e.g., Ref. [4]. While obviously $\eta_{cp}=1$ for $D=1$, the close-packed configuration for $D=2$ is a triangular lattice with $\eta_{cp} = \pi/(2\sqrt{3}) = 0.91$ and a face-centered-cubic lattice for $D=3$ with $\eta_{cp} = \pi/(3\sqrt{2}) = 0.74$. The latter structure is degenerate with respect to the stacking sequence. For higher dimensions, there is Minkowski's lower bound and Blichfeldt's upper bound [38] for η_{cp} , such that

$$\frac{\zeta(D)}{2^{D-1}} \leq \eta_{cp} \leq \frac{D+2}{2} \left(\frac{1}{\sqrt{2}} \right)^D \quad \text{for } D > 1, \quad (2)$$

where $\zeta(x)$ denotes the Riemann zeta function. The class of *laminated lattices* [38] is defined inductively and gives in general high packing fractions. The numerical values of η_{cp} are shown in Fig. 1 as a function of D . In particular, for $D < 25$, their packing is close to the upper bound, Eq. (2).

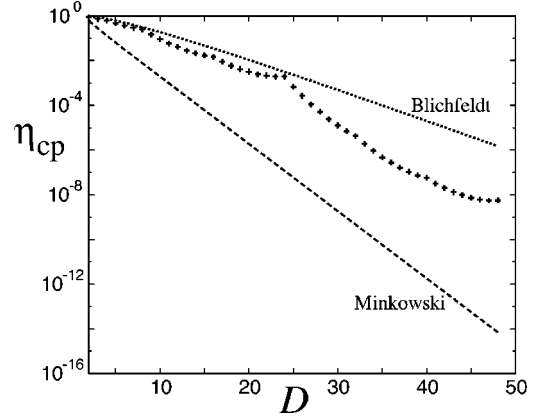


FIG. 1. Close-packing fraction η_{cp} as a function of dimensionality D . Blichfeldt's upper bound (dotted line), Minkowski's lower bound (dashed line), and the corresponding data for the laminated lattices (symbols) are shown. Note the logarithmic scale for η_{cp} .

Therefore, we restrict our investigation of the solid state to laminated lattices. However, as we shall show below, the general methodology can be applied to other crystals as well, provided their close-packing fraction is known.

III. FREE-VOLUME THEORY FOR THE SOLID STATE

We employ free-volume (or cell) theory in order to calculate free energies of the solid state. This approach, see e.g., [39], was also discussed for arbitrary D recently in Ref. [31]. Cell theory is based on the common partitioning of physical space into Wigner-Seitz cells (WSC) of the lattice structure under consideration. For hard spheres, no overlap between neighboring particles can occur, provided that each sphere stays completely within its WSC. Carrying out a partition sum where only this restricted set of configurations is taken into account strictly underestimates the full (exact) partition sum. In detail, let a denote the distance between nearest neighbors. The boundaries of the WSC are the distance $a/2$ apart from the lattice site. The spheres are supposed to stay completely within the WSC, such that each sphere center is allowed to move only a distance $a/2 - R$ from its lattice site towards a neighboring site. We assume that the shape of the accessible ("free") volume is the same as that of the WSC. Then the free volume of each sphere scales with the D th power of $(a - 2R)/a$, and we obtain

$$V_{\text{free}} = V_{\text{WS}} \left[\frac{a - 2R}{a} \right]^D. \quad (3)$$

If one relaxes the assumption of the same shape of free-volume cell and WSC, the real free volume is still larger than V_{free} . Let the free energy per particle be $f_s^{\text{exc}} + f^{\text{id}}$, where the ideal contribution is $f^{\text{id}} = \ln(\eta) - 1$. One obtains a strict upper bound for the excess free energy per particle of the solid state

$$\beta f_s^{\text{exc}} \leq 1 - D \ln \left[1 - \left(\frac{\eta}{\eta_{cp}} \right)^{1/D} \right]. \quad (4)$$

Note that if one inserts a lower bound for η_{cp} (as, e.g., for the laminated lattices considered in this paper) the resulting expression is still an upper bound for the free energy. An alternative for obtaining an estimate of the free energy is to calculate the free volume of each sphere with all the other spheres kept fixed. This allows each sphere to move twice as far from its lattice site as in the former approach. Of course, here one counts also forbidden configurations, so that the bounding property of the free energy is lost. However, in $D=3$ this gives a more accurate, albeit empirical estimate of the exact free energy. For general D , we obtain

$$\beta f_s^{\text{exc}} \approx 1 - D \ln \left[1 - \left(\frac{\eta}{\eta_{cp}} \right)^{1/D} \right] - D \ln 2. \quad (5)$$

IV. THEORIES FOR THE FLUID STATE

A. Virial expansion

Wyler, Rivier, and Frisch [24,10] have considered the Mayer series of the hard hypersphere fluid, and have shown that in the limit of infinite dimensionality, the virial expansion up to second order becomes asymptotically exact. The virial coefficients are defined by the expansion

$$\beta p = \rho + \sum_{n=2}^{\infty} B_n \rho^n, \quad (6)$$

where p is the pressure. The second virial coefficient is known analytically as $B_2 = 2^{D-1} V_D(R)$. The expansion of the excess free energy of the fluid state then reads

$$\beta f_f^{\text{exc}} = \frac{1}{2} \eta 2^D + \frac{1}{2} \frac{B_3}{[V_D(R)]^2} \eta^2 + O(\eta^3). \quad (7)$$

The third virial coefficient B_3 can be expressed by a quadrature [24] that can be solved analytically in even dimensions [26]. For odd dimensions we rely on a numerical solution. Our results for B_3 are shown versus D in Fig. 2. Although the numerical value of B_3 is quite large as $D \rightarrow \infty$, for small η its contribution to the free energy may become negligible. This is indeed the case for the densities relevant for freezing, as we will demonstrate below. We remark, however, that it is not proven that the virial expansion converges in the density region important for freezing [40]. There is thus still the possibility that the virial expansion does not describe the fluid state correctly. A similar situation exists in three dimensions, where the convergence of the virial expansion can only be proven rigorously up to $\eta \approx 0.02$ [40]. Numerical evaluation of the expansion to seventh order, however, show satisfactory results up to $\eta \approx 0.5$.

B. Percus-Yevick integral equation

Integral equations provide a very successful description of fluids. For hard spheres, the Percus-Yevick closure [41] is remarkably successful in three dimensions. One of its appealing properties is that it can be solved analytically for this system. Leutheusser generalized the solution to all odd dimensions $D = 2k + 1$, $k = 0, 1, 2, \dots$ [28] and solved the

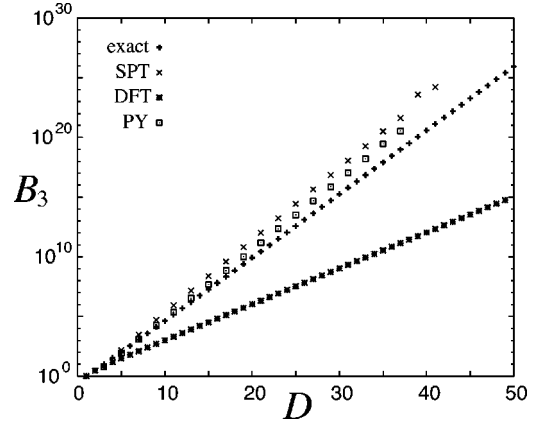


FIG. 2. Various approximations for the third virial coefficients B_3 as a function of dimension D . Shown is the exact result, as well as the results from scaled-particle theory (SPT), density-functional theory (DFT), and Percus-Yevick theory (PY).

equations explicitly for $D=1,3,5$. We follow his approach and treat the equations numerically for higher (odd) dimensions. We use the Wiener-Hopf factorization of the structure factor $S(q) = 1/[\tilde{Q}(q)\tilde{Q}(-q)]$, where q is the wave vector magnitude. Here $\tilde{Q}(q)$ is a regular function, which can be written as

$$\tilde{Q}(q) = 1 - (2\pi)^k \rho \int_0^{2R} Q(r) e^{ikr} dr. \quad (8)$$

It can be shown that $Q(r)$ is a polynomial of order $2k$ in r of the general form

$$Q(r) = (2R)^{2k} \sum_{n=0}^k Q_n \left(\frac{r}{2R} - 1 \right)^{n+k}, \quad 0 \leq r \leq 2R. \quad (9)$$

The system of integral equations can be reduced to a system of $k+1$ algebraic equations for the unknowns Q_0, \dots, Q_k . Two out of these equations are linear

$$(-1)^k = -k! 2^k Q_k + \rho (2\pi)^k (2R)^{2k+1} \times \sum_{n=0}^k (-1)^n \frac{Q_n}{(k+n+1)}, \quad k \geq 0, \quad (10)$$

$$(-1)^k = -(k-1)! 2^{k-1} Q_{k-1} + \rho (2\pi)^k (2R)^{2k+1} \times \sum_{n=0}^k (-1)^n \frac{Q_n}{(k+n+2)}, \quad k \geq 1, \quad (11)$$

and the remaining $k-1$ equations are nonlinear

$$Q^{(2n+1)}(0) = \frac{1}{2} \rho (2\pi)^k (-1)^{n+1} [Q^{(n)}(0)]^2 - \rho (2\pi)^k \times \sum_{\nu=0}^{n-1} (-1)^\nu Q^{(\nu)}(0) Q^{(2n-\nu)}(0), \quad 0 \leq n < k-1, \quad (12)$$

where $Q^{(k)}(0)$ denotes the k th derivative of $Q(r)$ at $r=0$. We solve Eqs. (10)–(12) numerically. As the effort quickly increases with rising dimension [we are faced with $(D+1)/2$ coupled equations], we restrict ourselves to $D \leq 33$. The function $Q(r)$ provides us with all the necessary information about the thermodynamics of the fluid state, as it is related to the contact value of the pair distribution function $g(r)$ of the hyperspheres via

$$g(2R^+) = (-1)^{k+1} Q^{(k)}(2R)/(2R)^{2k}, \quad (13)$$

which in turn determines the free energy via the virial route [28,41]

$$\beta p/\rho = 1 + 2^{D-1} \eta g(2R^+). \quad (14)$$

The second virial coefficient determined in this way is exact for any dimension. Formally expanding the solution into a power series with respect to η , we obtain the third virial coefficient numerically. As can be seen in Fig. 2, B_3 obtained in this way slightly overestimates the exact result.

C. Scaled-particle theory

The key idea of scaled-particle theory (SPT) [42] is to insert a spherical test particle of variable radius into a bulk fluid of hard spheres. The test particle is gradually expanded to the same size as the other spheres. One then obtains the free energy by thermodynamic integration of the virial equation. The key function by which all other properties can be expressed is $G(r)$, which is the contact value of the pair distribution function between test particle and the other spheres, if the radius of the test particle equals $r-R$.

In what follows, we generalize the SPT (which was originally developed for $D=3$) to arbitrary dimensions. The probability $p_0(r)$ of a spontaneous appearance of a cavity large enough to hold the test particle of radius r is directly connected to the work required in making it. This probability is equivalent to the probability of finding a spherical space with radius r unoccupied. By elementary statistical reasoning such as in $D=3$ [42], one obtains a relation between p_0 and $G(r)$, which is

$$\frac{1}{p_0(r)} \frac{dp_0(r)}{dr} = -\rho s_{D-1}(r) G(r). \quad (15)$$

If the cavity is so small that at most one sphere fits inside, i.e., $r \leq R$, the probability of finding this cavity unoccupied is clearly $p_0(r) = 1 - \rho V_D r^D$. Therefore,

$$G(r) = \frac{1}{1 - \rho V_D r^D} \quad \text{for } r \leq R. \quad (16)$$

Next we consider a cavity with radius $R < r < 2R/\sqrt{3}$. Then two, but not three spheres fit into the cavity. We have to correct for double-counting pairs, and obtain

$$p_0 = 1 - \rho V_D r^D + \int \int_{\text{cavity}} g(\mathbf{r}_1, \mathbf{r}_2) d\mathbf{r}_1 d\mathbf{r}_2 \quad (17)$$

$$= 1 - \rho V_D r^D + \frac{\rho^2}{2} \int_0^{2r} g(r') V_r(r') s_{D-1}(r') dr', \quad (18)$$

where $g(\mathbf{r}_1, \mathbf{r}_2)$ is the hypersphere pair distribution function and $r' = |\mathbf{r}_2 - \mathbf{r}_1|$; furthermore $V_r(r')$ denotes the overlap volume of two spheres with radius r at a distance r' . We will restrict ourselves in the following to odd dimensions $D = 2k+1$. From $g(r) = 0$ for $r < 2R$ it follows that p_0 is $k+1$ times continuously differentiable at $r=R$. Since $G(r)$ follows from $p_0(r)$ by differentiation [see Eq. (15)], $G(r)$ is k times continuously differentiable at $r=R$. Since we know the exact behavior of $G(r)$ for $r < R$, the first k derivatives of $G(r)$ at $r=R$ are also known.

A further constraint on $G(r)$ is obtained by noting that $G(\infty) = \beta p/\rho$ [42]. Equating with the virial expression for the pressure yields

$$1 + \frac{1}{2} 2^D \eta G(2R) = G(\infty). \quad (19)$$

Together with the $k+1$ values of the derivatives we have got $k+2$ constraints on $G(r)$. Next we expand $G(r)$ into a series in $1/r$,

$$G(r) = 1 + a_0 + \sum_{i=1}^{k+1} \frac{a_i}{(r/R)^i}. \quad (20)$$

This involves $k+2$ unknowns a_i , which must be chosen to fulfill

$$\frac{1}{1-\eta} = 1 + a_0 + \sum_{i=1}^{k+1} a_i, \quad (21)$$

$$\sum_{i=1}^{k+1} a_i (-1)^j \frac{(i+j-1)!}{(i-1)!} = \eta(1+a_0) \frac{D!}{(D-j)!} + \eta \sum_{i=1}^{k+1} a_i \frac{(D-i)!}{(D-i-j)!}, \quad (22)$$

$$a_0 = \frac{1}{2} 2^D \eta \left(1 + a_0 + \sum_{i=1}^{k+1} a_i 2^{-i} \right). \quad (23)$$

The first two sets of equations (21) and (22) are linear and can be used to express the a_1, \dots, a_{k+1} in terms of η and a_0 . The last Eq. (23) can then be turned into a quadratic equation for a_0 , which can be solved analytically. The non-linear equation (23) has to be solved numerically. From $a_0 = -1 + 1/G(\infty)$ we obtain directly the pressure [see Eq. (19)] and the equation of state. Decomposing the equation of state into a power law expansion with respect to density, we get the second and third virial coefficients. The second virial coefficient is exact. The third virial coefficient is shown as a function of spatial dimension D in Fig. 2. As in Percus-Yevick theory it is larger than the exact value.

It is possible to obtain the surface tension γ between a hard hypersphere fluid and a hard (hyper) planar wall via

SPT. In order to access γ , we consider the work required to form a cavity with a very large radius R , which can be expressed as

$$W(r) = pV_D(r) + \tilde{\gamma}s_{D-1}(r). \quad (24)$$

The quantity $\tilde{\gamma}$ is connected to the physical surface tension γ via the relation $\gamma = \tilde{\gamma} + pR$, compare, e.g., [43]. The probability $p_0(r)$ of observing a fluctuation containing such a cavity is further given by [10]

$$p_0(r) = \exp[-\beta W(r)]. \quad (25)$$

Hence, one finally obtains γ as a function of D and η as

$$\gamma = \frac{k_B T D}{s_{D-1}(R)} \eta \left(1 + a_0 - \frac{a_1}{D-1} \right), \quad (26)$$

which we will discuss as a function of D in Sec. VI.

V. DENSITY-FUNCTIONAL THEORY

Density-functional theory (DFT) has been very successful in describing inhomogeneous fluids in three dimensions [2]. It provides in principle a concept unifying the fluid and solid state within a single approach. For hard spheres, one particular approximation, the Rosenfeld functional, has the remarkable property of describing both the fluid state and the solid state very well incorporating the limit of close-packing correctly [44]. Within the Rosenfeld functional, or fundamental-measure theory, the nonlocal dependency of the excess free energy \mathcal{F} of the density ρ is treated via averages of the density over the sphere volume, surface, and other fundamental geometric measures [18]. The Rosenfeld functional may be formulated in such a way that it gives the correct zero-dimensional crossover [19,20]. The thermodynamics of a hard sphere system inside a cavity so small, that at most one sphere fits into it can be solved exactly. One obtains the excess free energy [19,20]

$$\beta\mathcal{F}^{(D=0)}[\rho] = \varphi_0(N) = N + (1-N)\ln(1-N), \quad (27)$$

where $0 \leq N \leq 1$ denotes the average number of particles inside the cavity. The same free energy is obtained from the Rosenfeld functional, if an external potential corresponding to the walls of the cavity is introduced. This provides a systematic way of deriving a similar DFT in arbitrary dimensions [21]. In the sequel we will work this out explicitly.

The general functional $\mathcal{F}[\rho]$ is assumed to be a sum of terms of the form

$$\beta\mathcal{F}[\rho] = \Phi_1^{(D)}[\rho] + \Phi_2^{(D)}[\rho], \quad (28)$$

$$\Phi_1^{(D)}[\rho] = \int d\mathbf{r} \varphi_1[\eta(\mathbf{r})] \int d\mathbf{R}_1 w_D(\mathbf{R}_1 - \mathbf{r}) \rho(\mathbf{R}_1), \quad (29)$$

$$\begin{aligned} \Phi_2^{(D)}[\rho] = & \int d\mathbf{r} \varphi_2 \eta(\mathbf{r}) \int d\mathbf{R}_1 \int d\mathbf{R}_2 \\ & \times w_D(\mathbf{R}_1 - \mathbf{r}) w_D(\mathbf{R}_2 - \mathbf{r}) P_D(\mathbf{R}_1, \mathbf{R}_2). \end{aligned} \quad (30)$$

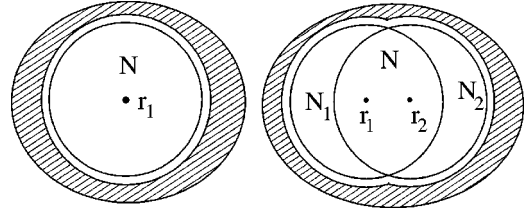


FIG. 3. Geometry of the two cavities used to derive the free energy functional $\mathcal{F}[\rho]$. Indicated are the possible positions of the sphere (r_1 or r_2) and the local packing fraction $\eta(r)$ within the respective region.

Here $\eta(\mathbf{r}) = \int d\mathbf{r}' \rho(\mathbf{r}') \Theta(R - |\mathbf{r}' - \mathbf{r}|)$ is the local packing density and $w_D(\mathbf{R}_1) = 1/s_{D-1}(R) \delta(R - |\mathbf{R}_1|)$ is a measure over the surface of the sphere. The integral kernel $P_D(\mathbf{R}_1, \mathbf{R}_2)$, therefore, couples densities averaged over the sphere surface. In order to make this functional unique we consider cavities of increasing complexity. These cavities are sketched in Fig. 3. A simple cavity capable of holding a sphere in just one place will uniquely determine $\varphi_1(\eta)$ and thus $\Phi_1^{(D)}[\rho]$. It turns out, however, that the exact free energy is not reproduced in a slightly more complicated cavity that can hold a sphere at either of two places. The requirement that the functional should give the analytically known value even in this case uniquely determines the functional form of $\varphi_2(\eta)$ and $P_D(\mathbf{R}_1, \mathbf{R}_2)$. This procedure has been invented (for $D=3$) in [21].

The simplest cavity is spherical, and just large enough to hold one sphere. The single particle density must then be $\rho(\mathbf{r}) = N \delta(\mathbf{r})$. The local packing density $\eta(\mathbf{r})$ equals N within a sphere of radius R and vanishes outside. Introducing the quantity $\eta_{R+\epsilon}(\mathbf{r}) = N \Theta(R + \epsilon - |\mathbf{r}|)$, we can write

$$\begin{aligned} \Phi_1^{(D)}[\rho] &= \int d\mathbf{r} \varphi_1[\eta(\mathbf{r})] \frac{1}{s_{D-1}(R)} \frac{\partial}{\partial \epsilon} \eta_{R+\epsilon}(\mathbf{r}) \Big|_{\epsilon=0} \\ &= \frac{1}{s_{D-1}(R)} \frac{\partial}{\partial \epsilon} \int d\mathbf{r} F[\eta_{R+\epsilon}(\mathbf{r})] \Big|_{\epsilon=0} \\ &= \frac{1}{s_{D-1}(R)} \frac{\partial}{\partial \epsilon} F(N) V_D(R + \epsilon) \Big|_{\epsilon=0} \\ &= F(N), \end{aligned} \quad (31)$$

with F denoting the integral of φ_1 . Comparing this with the correct zero dimensional limit, one gets

$$\Phi_1^{(D)}[\rho] = \int d\mathbf{r} \varphi_1[\eta(\mathbf{r})] \int d\mathbf{R}_1 w_D(\mathbf{R}_1 - \mathbf{r}) \rho(\mathbf{R}_1), \quad (32)$$

with $\varphi_1(\eta) \equiv \partial \varphi_0(\eta) / \partial \eta = -\ln(1-\eta)$.

Consider another cavity with $\rho(\mathbf{r}) = N_1 \delta(\mathbf{r} - \mathbf{r}_1) + N_2 \delta(\mathbf{r} - \mathbf{r}_2)$, $N = N_1 + N_2 \leq 1$, and $r_{12} = |\mathbf{r}_1 - \mathbf{r}_2| \leq 2R$. For this kind of cavity the first term $\Phi_1^{(D)}$ of the free energy functional derived above does not give the correct free energy $\varphi_0(N)$ but

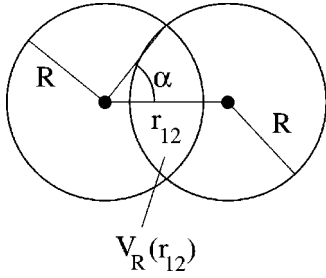


FIG. 4. Geometrical interpretation of $V_R(r_{12})$ as the overlap volume of two spheres of radius R with distance r_{12} .

$$\Phi_1^{(D)}[\rho] = \varphi_0(N) - \xi(r_{12})[\varphi_0(N) - \varphi_0(N_1) - \varphi_0(N_2)], \quad (33)$$

$$\begin{aligned} \xi(r_{12}) &= 1 - \frac{1}{s_{D-1}(R)} \frac{\partial}{\partial \epsilon} V_{R+\epsilon}(r_{12}) \Big|_{\epsilon=0} \\ &= 1 - \frac{V_{D-1}}{DV_D} (D-1) I_{D-2}(\alpha), \end{aligned} \quad (34)$$

$$I_D(\alpha) = \int_0^\alpha \sin^D(\varphi) d\varphi, \quad (35)$$

$$R \cos(\alpha) = r_{12}/2. \quad (36)$$

$V_{R+\epsilon}(r_{12})$ denotes the overlap volume of two spheres of radius $R+\epsilon$ at a distance r_{12} , see the sketch in Fig. 4.

We next determine the second contribution $\Phi_2^{(D)}[\rho]$ so that the deviation of the free energy from the exact zero-dimensional limit is corrected for. We obtain

$$\begin{aligned} \Phi_2^{(D)}[\rho] &= \int d\mathbf{r} \varphi_2[\eta(\mathbf{r})] \int d\mathbf{R}_1 w_D(\mathbf{R}_1 - \mathbf{r}) \rho(\mathbf{R}_1) \\ &\quad \times \int d\mathbf{R}_2 w_D(\mathbf{R}_2 - \mathbf{r}) \rho(\mathbf{R}_2) P(\mathbf{R}_1, \mathbf{R}_2), \end{aligned} \quad (37)$$

with

$$\xi(r_{12}) = 1 - \frac{V_{D-1}}{DV_D} (D-1) I_{D-2}(\alpha), \quad (38)$$

$$\begin{aligned} P_D(r_{12}) &= \frac{\xi(r_{12}) D^2 V_D^2 r_{12}^2}{V_{D-1} R^D (D-1) \sin^{D-3}(\alpha) \cos(\alpha)} \\ &\quad \text{for } r_{12} \leq 2R, \end{aligned} \quad (39)$$

$$\varphi_2(\eta) = \frac{\partial \varphi_1(\eta)}{\partial \eta} = \frac{1}{1-\eta}. \quad (40)$$

This completes the prescription of our functional. In principle, one could go further, and consider cavities that enforce δ density distributions composed of three or more δ spikes. Indeed in the case $D=3$ [21], up to *three* δ spikes were considered. One might speculate that up to D δ spikes should

be necessary in D dimensions. Due to the geometrical complexity, we have not followed this (albeit desirable) route in the present work.

For the homogeneous phase the integrals in Eq. (40) can be evaluated analytically. One obtains for the excess free energy per particle

$$f_f^{\text{exc}} = \varphi_1(\eta) + \frac{1}{2} \eta \varphi_2(\eta) (2^D - 2), \quad (41)$$

which we will also use as an estimate for the fluid free energy. Expanding into a power series with respect to η , one obtains

$$f_f^{\text{exc}} = \frac{1}{2} 2^D \eta + \frac{1}{2} (2^D - 1) \eta^2 + O(\eta^3), \quad (42)$$

hence, the correct second virial coefficient is reproduced by our density functional. The third virial coefficient is shown versus D in Fig. 2. It is significantly smaller than the exact result. We attribute this failure to the restricted set of cavities considered. (Note that in $D=3$ three δ spikes are needed to get B_3 correctly.) However, our functional has all terms that are important near close packing in $D=3$ [44], and we believe that this holds also for $D>3$. We further emphasize that this functional has much more predictive power than just giving the equation of state of the fluid. In principle, it could further be used to derive structural fluid correlations and inhomogeneous situations including freezing. We have not considered such applications here but leave them for future studies.

VI. RESULTS AND DISCUSSION

With the theories described above, we calculated freezing/melting coexistence densities using Maxwell's double tangent construction. We find a first-order freezing transition occurring at densities well below close packing. In Fig. 5, we plot the coexisting fluid (η_f) and solid (η_s) packing fractions obtained by using either third-order virial expansion or scaled-particle theory for the fluid and free-volume theory with unfixed neighbors [Eq. (4)] for the solid as a function of dimension D . Close-packing fractions η_{cp} are included for comparison. It might seem from this graph that the fluid and solid coexisting densities are not affected very much by the variation of the close-packed density with dimension but this is due to the logarithmic density scale.

We note that the coexistence densities do only depend weakly on the particular solid state theory for large D . If the virial expansion up to third order is used for the fluid free energy (Fig. 5), a freezing transition shows up for $D>11$. On the other hand, Percus-Yevick, scaled-particle and density-functional theory (all of which are more reliable for smaller dimensionalities) result in a freezing transition at any $D \geq 3$. We have compared our theoretical results to computer simulation data in the special cases $D=3,5$ [32], (see Table I). For $D=5$, we find reasonable agreement within the statistical error of the simulation.

The agreement between the different fluid state theories becomes better with increasing dimensionality. This is expected, since the virial expansion becomes exact for $D \rightarrow \infty$ and all our approaches reproduce the exact second virial co-

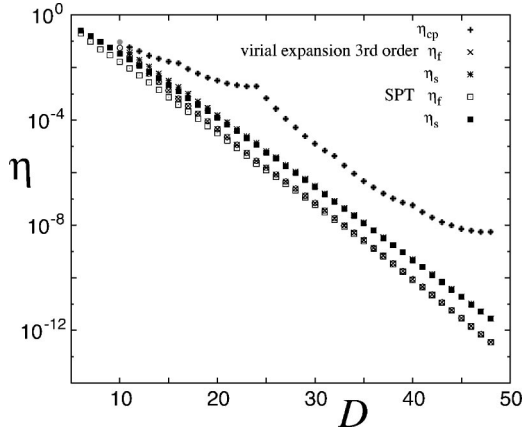


FIG. 5. Fluid (η_f) and solid (η_s) coexistence packing fractions and the close packing fraction η_{cp} of the corresponding laminated lattice versus dimension D .

efficient. The relative density jump in the coexistence densities, $(\eta_s - \eta_f)/\eta_s$, is plotted against dimension in Fig. 6. This quantity approaches its maximal value of unity for large D . That implies that the transition is strongly first order. On the basis of our data we conclude that $\eta_s/\eta_{cp} \rightarrow 0$ and $\eta_f/\eta_s \rightarrow 0$, for large D .

Let us discuss the relation of this theory to a perturbative analysis based on the Kirkwood spinodal instability of the fluid. A second-order freezing transition was predicted [23] in the case of first taking the limit $D \rightarrow \infty$ and then taking the thermodynamical limit. For finite D the instability density has been worked out explicitly by Frisch and Percus [23] as

$$\eta \approx 0.871(e/8)^{D/2} D^{1/6} e^{1.473D^{1/3}}. \quad (43)$$

Bagchi and Rice [13] found the same functional dependence on D , but a different prefactor such that

$$\eta \approx 0.239(e/8)^{D/2} D^{1/6} e^{1.473D^{1/3}}. \quad (44)$$

These densities are compared to our fluid coexisting densities based on the virial expansion and free-volume theory in Fig. 7. Our η_f are smaller than the instability densities. This implies that the fluid instability is preempted by first-order freezing at all high dimensions such that the Kirkwood in-

TABLE I. Results for the coexistence densities η_f, η_s for small dimensionality $D=3$ and 5 obtained from cell theory (CT) with fixed and unfixed neighbors compared to simulation results. We estimated the simulation values for $D=5$ from the results given in Ref. [32].

D	Method	η_f	η_s	η_{cp}
3	CT, unfixed			0.74048
	CT, fixed	0.562138	0.601772	
	simulation	0.494	0.545	
5	CT, unfixed	0.27353	0.348053	0.465258
	CT, fixed	0.202184	0.258753	
	simulation [32]	≈ 0.19	≈ 0.29	

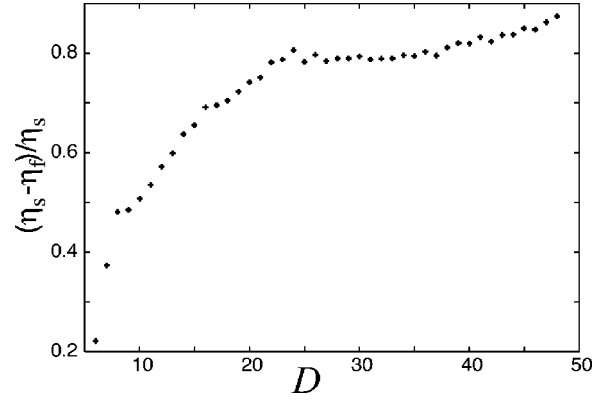


FIG. 6. Relative jump in coexistence densities $(\eta_s - \eta_f)/\eta_s$ versus dimension D .

stability only applies for a metastable fluid. This has indeed been suggested in a recent paper by Frisch and Percus [16], where relevant diagram resummations are carried out before taking the limit $D \rightarrow \infty$ resulting in a prior spinodal. The authors suggest that “at a density less than that of the Kirkwood, a first-order transition intervenes.” Provided the virial expansion approaches exactness (as assumed in the instability analysis of Refs. [13,24]) [45], our analysis indicates a first-order phase transitions for large dimensions, because the free-volume theory provides a strict upper bound for the solid free energy (see Sec. III), which means that the real coexisting fluid density can only be smaller than in our calculation. As an aside, we apply the same analysis to hard *hypercubes* and find a qualitatively different result. The instability densities as calculated analytically by Kirkpatrick [9] are smaller than the coexisting densities obtained from our analysis. This implies that for hard hypercubes the fluid instability can be real. Of course, this system is qualitatively different from hard hyperspheres. The close-packing fraction of hard hypercubes is unity, independent of dimension, and the fluid is anisotropically ordered due to the fixed orientations of the particles. Apparently, this makes it easier for the solid to step in via a second-order phase transition.

The Lindemann parameter is defined via L

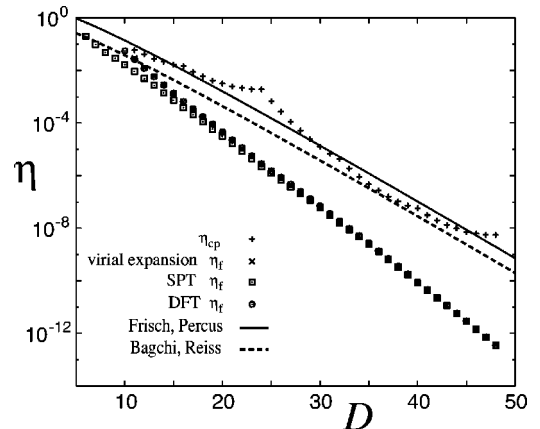


FIG. 7. Comparison of the freezing densities η_f from different theories against the Kirkwood instability density obtained by Frisch and Percus [Eq. (43)] and Bagchi and Reiss [Eq. (44)].

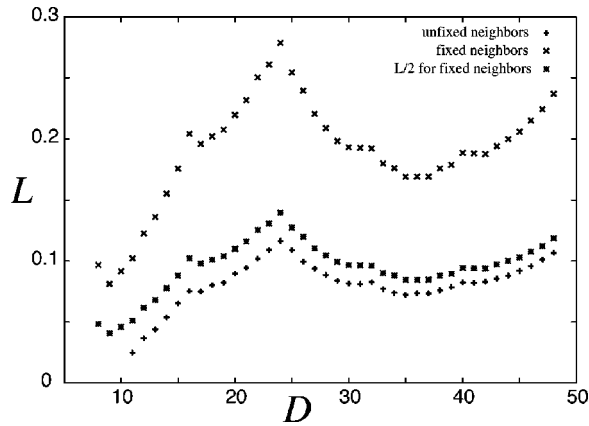


FIG. 8. Lindemann parameter L at melting as a function of dimension D .

$= \sqrt{\langle (\Delta \vec{r})^2 \rangle} / a$ as the ratio between the root-mean-square displacement of a particle in the solid and the lattice constant a . Three-dimensional crystal melting is accompanied by a Lindemann parameter of roughly 0.1. We test this rule [46] within our theory for arbitrary D in Fig. 8. Free-volume theory, where we assume a constant density profile within the free volume cell, can be used to estimate L . We have used approaches with both unfixed and fixed nearest neighbors. The main effect of using the fixed nearest neighbors approach is a doubling of the available space for the spheres in each direction. If the coexistence densities were the same, the difference in L between the fixed and unfixed approach would be a factor of 2. However, if the approach with the fixed nearest neighbors is used, the solid coexistence densities η_s change slightly, leading to a different a in L . Data for L at coexistence are presented in Fig. 8. For the fluid state we have used the virial expansion. The difference in L between the approaches using unfixed and fixed nearest neighbors are nearly a factor of 2. Within cell theory the Lindemann parameter at coexistence does not vary dramatically from its threshold value of 0.1, valid in three dimensions, and it is rather insensitive to the dimensionality. The data for L obtained within the fixed neighbor approach show that the result is stable (up to a trivial factor of 2) with respect to a different solid state theory. Thus the crude melting rule also holds in higher spatial dimensions. The Lindemann criterion is thus pretty robust. Note that it is also valid for $D=2$, provided the relative mean-square displacement [47] is used. Furthermore it holds in $D=3$ even for interfacial freezing [48] and freezing of polydisperse spheres both in equilibrium and nonequilibrium [49].

We finally show, as a side product, the wall-fluid tension γ of hard hyperspheres, as given by Eq. (26). In Fig. 9, we plot γ for a fixed scaled packing fraction $\eta = 2^{2-D}$ versus dimensionality D . This packing fraction is close to bulk freezing. For this choice of parameters, γ increases with D . Note that in three dimensions, the scaled-particle expression was found to be in very good agreement with computer simulations [43] and density-functional studies [50] for any packing fraction up to freezing.

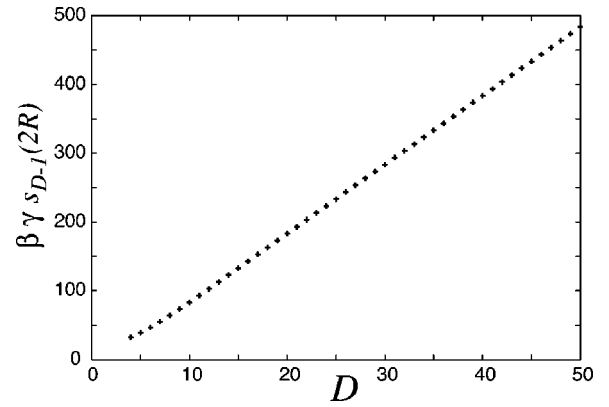


FIG. 9. Reduced surface tension $\beta \gamma_{S_{D-1}}(2R)$ according to scaled-particle theory as a function of the dimension D at the respective density $\eta = 4/2^D$, which is close to freezing.

VII. CONCLUSIONS

In conclusion, we have studied the fluid and solid free energies for hard hyperspheres. We have generalized scaled-particle theory to arbitrary dimensions and solved the Percus-Yevick liquid integral equation theory numerically in odd dimensions up to $D=33$. We have further proposed a free energy density functional for an inhomogeneous hard hypersphere fluid for arbitrary dimension. Assuming laminated lattice structures for the solid, we have used free-volume theory for the solid that provides a strict upper bound to the free energy. As a result, we find a first-order freezing transition where the density jump approaches the solid coexistence density as D grows. We have shown that this first-order freezing transition preempts the second-order Kirkwood spinodal instability of the fluid.

We point out that computer simulations are needed for $D > 3$ in order to improve the statistics of the simulations done for $D=4,5$ [32] and to explore the fluid-solid phase boundaries for $D > 5$. The numerical effort for such simulations, however, increases rapidly with dimension, as the number of particles in a hypercubic box (with periodic boundaries) increases significantly with D .

It would also be interesting to access hypersphere freezing by the unifying concept of density functional theory. The fluid free energy was derived in this paper. To get the solid free energy, one could use an ansatz based on Gaussian density peaks centered on a (laminated or any other) lattice and minimize the free energy with respect to the width of the peaks and the lattice structure. One could further extract the wall-fluid and wall-solid surface tensions from DFT. We leave these problems for further studies.

ACKNOWLEDGMENTS

We thank Y. Rosenfeld and J.-P. Hansen for helpful remarks, and T. White for proofreading the manuscript.

- [1] D.W. Oxtoby, *Nature (London)* **347**, 725 (1990).
- [2] H. Löwen, *Phys. Rep.* **237**, 249 (1994).
- [3] D. Frenkel, *Physica A* **263**, 26 (1999).
- [4] For a review and related references, see H. Löwen, in *Spatial Statistics and Statistical Physics*, edited by K. Mecke and D. Stoyan, Springer Lecture Notes in Physics Vol. 554 (Springer, Berlin, 2000), p. 295.
- [5] P.G. Bolhuis, D. Frenkel, S.-C. Mau, and D.A. Huse, *Nature (London)* **388**, 235 (1997).
- [6] W.G. Hoover, and F.H. Ree, *J. Chem. Phys.* **49**, 3609 (1968).
- [7] A. Jaster, *Europhys. Lett.* **42**, 277 (1998); *Phys. Rev. E* **59**, 2594 (1999).
- [8] L. Tonks, *Phys. Rev.* **50**, 955 (1936).
- [9] T.R. Kirkpatrick, *J. Chem. Phys.* **85**, 3515 (1986).
- [10] H.L. Frisch, N. Rivier, and D. Wyler, *Phys. Rev. Lett.* **54**, 2061 (1985).
- [11] M. Schulz, and H.L. Frisch, *Phys. Rev. E* **52**, 442 (1995).
- [12] F.H. Stillinger *J. Chem. Phys.* **70**, 4067 (1979).
- [13] B. Bagchi and S.A. Rice, *J. Chem. Phys.* **88**, 1177 (1988).
- [14] R.P. Sear and B.M. Mulder, *Mol. Phys.* **93**, 181 (1998).
- [15] K.K. Mon and J.K. Percus, *J. Chem. Phys.* **11**, 2734 (1999).
- [16] H.L. Frisch and J.K. Percus, *Phys. Rev. E* **60**, 2942 (1999).
- [17] Y. Rosenfeld, *Phys. Rev. Lett.* **63**, 980 (1989).
- [18] For a review, see Y. Rosenfeld, *Mol. Phys.* **94**, 929 (1998).
- [19] Y. Rosenfeld, M. Schmidt, H. Löwen, and P. Tarazona, *J. Phys.: Condens. Matter* **8**, L577 (1996).
- [20] Y. Rosenfeld, M. Schmidt, H. Löwen, and P. Tarazona, *Phys. Rev. E* **55**, 4245 (1997).
- [21] P. Tarazona, Y. Rosenfeld, *Phys. Rev. E* **55**, R4873 (1997).
- [22] W. Klein, H.L. Frisch, *J. Chem. Phys.* **84**, 968 (1986).
- [23] H.L. Frisch, and J.K. Percus, *Phys. Rev. A* **35**, 4696 (1987).
- [24] D. Wyler, N. Rivier, and H.L. Frisch, *Phys. Rev. A* **36**, 2422 (1987).
- [25] Y. Elskens, and H.L. Frisch, *Phys. Rev. A* **37**, 4351 (1988).
- [26] M. Luban, and A. Baram, *J. Chem. Phys.* **76**, 3233 (1982).
- [27] L.E. González, D.J. González, and M. Silbert, *J. Chem. Phys.* **97**, 5132 (1992).
- [28] E. Leutheusser, *Physica A* **127**, 667 (1984).
- [29] E.S. Velazquez, L. Blum, H.L. Frisch, *J. Stat. Phys.* **89**, 203 (1997).
- [30] G. Parisi, and F. Slanina, *Phys. Rev. E* **62**, 6554 (2000).
- [31] E. Velasco, L. Mederos, and G. Navascues, *Mol. Phys.* **97**, 1273 (1999).
- [32] J.P.J. Michels, and N.J. Trappeniers, *Phys. Lett. A* **104**, 425 (1984).
- [33] J.L. Colot, and M. Baus, *Phys. Lett. A* **119**, 135 (1986).
- [34] A. Santos, S.B. Yuste, and M. López de Haro, *Mol. Phys.* **96**, 1 (1999).
- [35] S.B. Yuste, A. Santos, and M. López de Haro, *Europhys. Lett.* **52**, 158 (2000).
- [36] A. Santos, *J. Chem. Phys.* **112**, 10 680 (2000).
- [37] M. Bishop, A. Masters, and J.H.R. Clarke, *J. Chem. Phys.* **110**, 11 449 (1999).
- [38] C. A. Rogers, *Packing and Covering* (Cambridge University Press, Cambridge, 1964).
- [39] A. Münster, *Statistical Thermodynamics*, (Springer-Verlag, Berlin, 1974), Vol. II, pp. 337–346.
- [40] J. Groeneveld, *Phys. Lett.* **3**, 50 (1962).
- [41] J. -P. Hansen and I. R. McDonald, *Theory of Simple Liquids*, 2nd ed. (Academic Press, New York, 1986).
- [42] H. Reiss, H.L. Frisch, and J.L. Lebowitz, *J. Chem. Phys.* **31**, 369 (1959).
- [43] M. Heni, and H. Löwen, *Phys. Rev. E* **60**, 7057 (1999).
- [44] B. Groh, and B. Mulder, *Phys. Rev. E* **61**, 3811 (2000).
- [45] An even less severe assumption is that the second-order virial free energy is a lower bound to the exact free energy. Although this is physically plausible (and confirmed in $D=3$), we are not aware of a strict mathematical proof of this assumption and leave it as an open question.
- [46] F.A. Lindemann, *Phys. Z.* **11**, 609 (1910).
- [47] K. Zahn, and G. Maret, *Phys. Rev. Lett.* **85**, 3656 (2000).
- [48] M. Heni, and H. Löwen, *J. Phys.: Condens. Matter* **13**, 4675 (2001).
- [49] H. Löwen, and G.P. Hoffmann, *Phys. Rev. E* **60**, 3009 (1999).
- [50] B. Götzelmann, A. Haase, and S. Dietrich, *Phys. Rev. E* **53**, 3456 (1996).